Ultrasensitive Optofluidic Surface-Enhanced Raman Scattering Detection with Flow-through Multihole Capillaries

Yunbo Guo,[†,§] Maung Kyaw Khaing Oo,[†,§] Karthik Reddy,[†,‡] and Xudong Fan[†,*]

[†]Department of Biomedical Engineering and [‡]Department of Electrical Engineering and Computer Science, University of Michigan, Ann Arbor, Michigan 48109, United States [§]These authors contributed equally to this work.

ABSTRACT

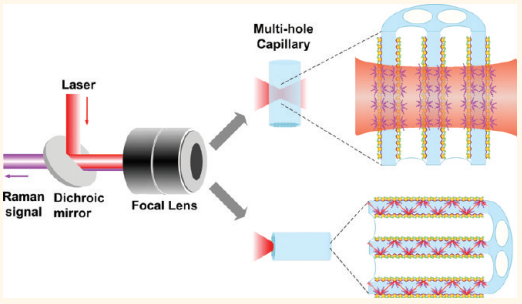

3-Dimensional surface-enhanced Raman scattering (SERS) detection integrated with optofluidics offers many advantages over conventional SERS conducted under planar and static conditions. In this paper, we developed a novel optofluidic SERS platform based on nanoparticle-functionalized flow-through multihole capillaries for rapid, reliable, and ultrasensitive analyte detection. The unique configuration not only provides 3-dimensional geometry for significantly increased SERS-active area and inherent fluidic channels for rapid and efficient sample delivery, but also confines and transmits light along the capillary for large SERS signal accumulation. Using a capillary consisting of thousands of micrometer-sized holes adsorbed with gold nanoparticles, we investigated the proposed optofluidic SERS system using the transverse and longitudinal detection methods, where the SERS excitation and collection were perpendicular to and along the capillary, respectively. A detection limit better than 100 fM for rhodamine 6G was achieved with an enhancement factor exceeding 10^8.

KEYWORDS: optofluidics · surface-enhanced Raman scattering · flow-through · multihole capillary · microstructured optical fiber · gold nanoparticle

Since its discovery in the 1970s,[1,2] surface-enhanced Raman scattering (SERS) has shown tremendous potential for bio/chemical molecular analysis at the trace and even single molecule level.[3−6] Traditionally, SERS detection is performed on single planar SERS-active surfaces, which are prepared by fabricating nanostructures (nanodomes,[7] nanoantenna,[8] metal-capped nanopillars,[9] nanoporous silicon,[10] and gold,[11,12] *etc.*) on planar substrates (such as silicon wafers) using nanoparticle self-assembly, lithography, nanoimprint, etching, or annealing. However, due to the 2-dimensional (2-D) configurations, the available density of SERS-active sites within the detection volume is limited. Additionally, the 2-D SERS substrates rely on the analytes in bulk solution to diffuse slowly to the SERS-active sites. Therefore, the corresponding SERS detection is time-consuming and unfavorable for fast, in-line, real-time analysis with low sample consumption.

Optofluidics is an emerging field that synergistically integrates optics and microfluidics to significantly enhance the performance of various existing detection techniques, including SERS.[13−18] In the past few years, a number of optofluidic SERS platforms have been investigated.[17,18] For example, photonic crystal fibers (PCFs),[19−23] consisting of a central hollow or solid core surrounded by many air holes, offer inherent fluidic channels for convenient flow-through analyte delivery. In addition, the excitation light and Raman-scattered photons can propagate along the entire length of the PCFs, enabling 3-D SERS detection with much larger detection area (and hence higher sensitivity) than the 2-D planar SERS substrates. A detection of 100 pM for rhodamine 6G (R6G) was reported by using either the hollow central core or holey cladding of a PCF as the microfluidic channel and the adsorbed silver nanoparticles as the SERS-active sites.[21,22] An on-chip optofluidic SERS system was also implemented using an antiresonant reflecting optical waveguide (ARROW) structure, which demonstrated a detection sensitivity to a minimum concentration of 30 nM of R6G molecules adsorbed to

* Address correspondence to xsfan@umich.edu.

Received for review September 29, 2011 and accepted December 18, 2011.

Published online December 18, 2011
10.1021/nn203733t

silver nanoparticles.[24] Porous aluminum membranes,[25,26] benefiting from both large SERS-active surface of hundreds of nanochannels within the detection volume and waveguiding capability along the 60 μm long nanochannels, have achieved pico- or zeptogram-level detection of explosives. In addition, step microfluidic-nanochannel junctions were utilized to concentrate analytes and/or analyte−nanoparticle aggregates near the inlet of the narrow nanochannels, and achieved a detection limit ranging from 3 fM for Cu/Zn-superoxide dismutase aggregates[27] to 10 pM for adenine molecules.[28] Nanoporous materials have also been explored to develop 3-D optofluidic SERS devices. Liu *et al*. adopted a nanoporous polymer monolith within a microfluidic channel to trap and concentrate silver nanoclusters in a 3-D matrix, which greatly enhanced the SERS intensity and achieved a detection limit of 220 fM for R6G.[29] While significant progress has been made in 3-D optofluidic SERS systems, they still experience either relatively low limited sensitivity,[21,22,24,28] complicated and costly device fabrication procedures,[24,27,28] short interaction length unfavorable for large signal accumulation or in-line analyte monitoring,[25,26,29] difficulties in controlling metallic nanoparticle aggregations and nanoclusters,[28,29] or time-consuming SERS substrate (*i.e*., metallic nanoparticle) deposition and analyte accumulation processes.[22,27] How to achieve a robust, simple, reliable, highly sensitive, and cost-effective optofluidic SERS platform still remains unanswered.

To address the above challenges, here we developed a flow-through 3-D optofluidic SERS platform based on micro/nanostructured capillaries, as shown in Figure 1. Metallic nanoparticles can be predeposited on the inner surface of each micro/nanofluidic channel before the analyte is flowed through. Or they can be premixed with the analyte before being injected into the capillary and subsequently deposited on the inner surface of the channels. The detection can be carried out in two configurations, transverse and longitudinal detections, where the SERS excitation and collection are perpendicular to and along the capillary, respectively, as illustrated in Figure 1. Both of the detection configurations provide unique advantages. In the transverse method, the SERS signal is from the SERS-active sites within the detection volume determined by the laser excitation and the SERS collection optics. Owing to the extremely large surface resulting from thousands of micro/nanosized holes in the capillary, 3-D sensitive SERS detection can be achieved. In addition, the inherent flow-through channels enable robust and reliable metallic nanoparticle immobilization, and fast and convenient analyte delivery. Moreover, the flow-through capillary with micro/nanosized holes combines convective flow and short diffusion length scales, which significantly reduces the time required for analytes to reach the SERS-active surface and

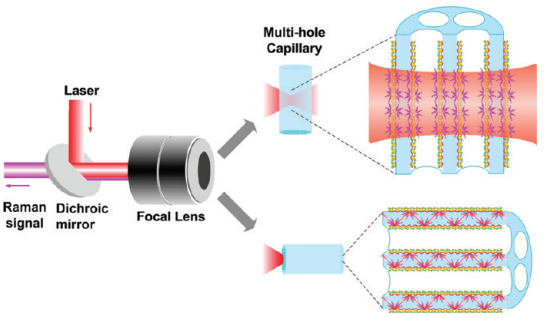

Figure 1. Schematic of a flow-through optofluidic Raman system based on a multihole capillary. The SERS excitation and detection are arranged transversely (top) or longitudinally (bottom) with respect to the capillary.

increases the analyte capture efficiency.[30−32] Furthermore, measurement in the transverse direction enables in-line SERS detection, which is favorable for real-time measurement and miniaturized system integration. In contrast, the porous aluminum membrane[25,26] is not able to operate in the transverse direction restricted by its short available length (~60 μm). The longitudinal detection method takes additional advantage of SERS signal accumulation along the capillary. The excitation light is guided within the wall (silica) *via* total internal reflection (especially within the triangular junctions formed by three holes along the capillary[22,33,34]) and quasi-guided by the hole *via* multireflection.[33] The SERS generated by the excitation light is then coupled back to and guided by the wall and hole. As a result, the SERS signal accumulates along the capillary but also experiences progressive loss due to the scattering/absorption of gold nanoparticles. Therefore, the overall backward or forward propagating SERS intensity is expected to be the sum of the SERS signal gain and its scattering/absorption loss over the whole capillary length.[23] Consequently, the well-defined flow-through micro/nanochannels are able to increase the SERS accumulative length as a PCF does, a distinct advantage over the short-length porous aluminum membrane and nonwaveguiding porous polymer monolith.[29] In addition, in contrast to the hollow-core PCFs where the SERS-active area is limited to the central aqueous guided hollow core as light is tightly confined there by precisely arranged surrounding holes,[20,21,23] the multihole capillary described here does not have photonic confinement and each hole (or channel) can work independently as the SERS-active substrate. Therefore, the excitation light can be at any wavelength and can reach all channels within the capillary, which greatly increases the sensing surface area. It also makes the multihole capillary quite different from the solid-core PCFs where a solid central core is surrounded by well-arranged periodic hole array.[19,22,35] Although their effective index guided core enables them to operate over all wavelengths, the fundamental guided mode concentrates most of the input light energy in the solid core,

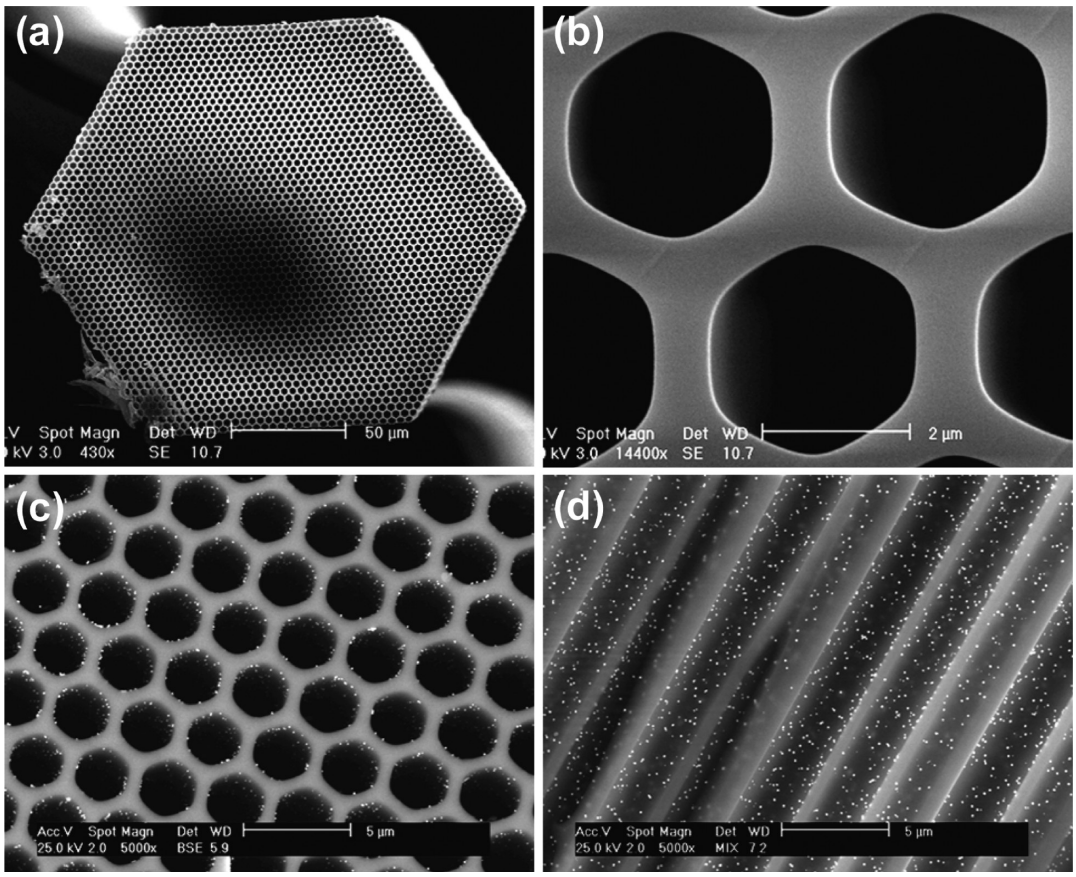

Figure 2. (a) Scanning electron microscopy (SEM) images of the multihole capillary with the outer diameter of 190 μm, hole size of 2.9 μm, and wall thickness of 0.7 μm; (b) enlarged images of the holes; (c) facet of the capillary adsorbed with gold nanoparticles; (d) cross section of flow channels with adsorbed gold nanoparticles.

and only a small portion of the energy in the aqueous regions surrounding the core is available as the evanescent field to interact with metal nanoparticles for Raman enhancement. Moreover, both hollow-core and solid-core PCFs normally need long fiber length (a few to tens of centimeters) to achieve large SERS signal, which increases the difficulty of immobilizing metal nanoparticles onto the inner surface of the PCFs.[19,23] However, as shown below, the multihole capillary can achieve a large signal with a short length less than 3 mm, greatly simplifying the nanoparticles immobilization process. Furthermore, the multihole capillary does not require delicate effort to arrange the holes to construct the photonic crystal structure or periodic hole array, and therefore, it can be fabricated with the same fiber drawing method as for PCFs, but more easily and more cost-effectively.

In this paper, we used a multihole capillary with micrometer-sized flow-through 2700 holes and 117 nm gold nanoparticles as a model system to demonstrate the flow-through 3-D optofluidic SERS platform. Both transverse and longitudinal detections were investigated. Ultrasensitive SERS detection of low concentrations of R6G molecules adsorbed on discrete gold nanoparticles was achieved with a detection limit better than 100 fM, a sampling time less than 5 min, and a data acquisition time of 2 s.

RESULTS AND DISCUSSION

The flow-through multihole capillaries used in our experiments were 190 μm in outer diameter and had 2700 uniform 2.9-μm holes with 0.7-μm thick wall between two adjacent holes (see Figure 2a,b). They were fabricated using an in-house computer controlled fiber/capillary drawing system and a borosilicate glass preform (1.30 mm outer diameter and 18 μm hexagonal holes).

Transverse Detection. We first investigated the proposed SERS platform using the transverse detection method. All Raman and SERS measurements were carried out with the customized Raman spectroscopy system where the probe beam from a 785 nm diode laser was focused by using an aspheric lens (NA = 0.55 and f = 4.51 mm) to produce a spot size of approximately 3 μm in diameter with 6 mW of optical power. The effective detection volume is approximately 850 μm^3 (*i.e.*, 0.85 pL) which is determined by the excitation laser spot size and Raman signal collection optics (120 μm collection depth across the capillary) (see Figure S1 in Supporting Information). Since the

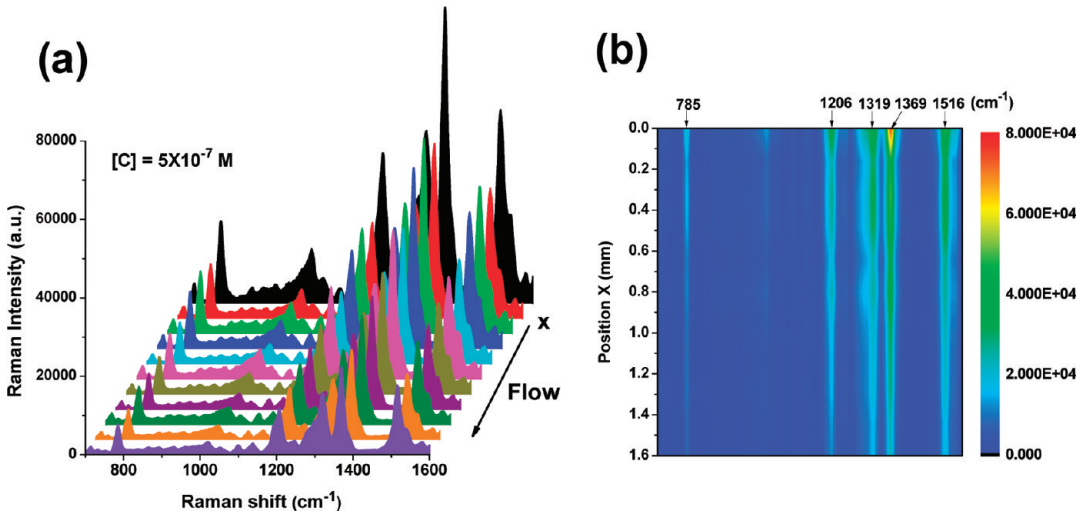

Figure 3. (a) Series of SERS spectra for 5 $\times$ 10^{-7} M R6G obtained by the stepwise measurement along the capillary in an increment of 160 μm. All spectra were acquired using the transverse detection method with 6 mW of excitation power and 2 s of integration time, with no postdata processing except for a 5-point adjacent-averaging smooth. (b) SERS intensity distribution along the capillary extracted from panel a.

multihole capillary provides a very large surface-to-volume ratio of 0.87 μm^{-1}, the total effective illuminated surface area is estimated to be 740 μm^2, over 2 orders of magnitude larger than 7 μm^2 obtained with a single flat surface using the same excitation and collection optics.

The multihole capillary with micrometer-sized flow channels also enables metallic nanoparticles to be immobilized onto the inner surface as SERS-active sites. Here we intentionally chose large-sized gold nanoparticles as they have high scattering efficiency and thus produce high SERS intensity.[36] In the experiments, gold nanoparticles with a diameter of 117 $\pm$ 20 nm were employed, which were synthesized by the modified UV-assisted photochemical method as described previously.[36] They had a resonance wavelength of 570 nm (see Figure S2 in Supporting Information) and achieved an enhancement factor over 10^6 in SERS measurements.[36] Immobilization of gold nanoparticles onto the inner surface of the capillary was achieved through polyelectrolyte mediation. First, poly(allylamine hydrochloride) (PAH) was flowed through a long capillary ($\sim$20 mm) and allowed to adsorb on the channel surface, providing anchoring sites for gold nanoparticles. Then, a 3 mm long portion of the PAH-treated capillary was cut and mounted on a needle connected to a syringe. Gold nanoparticles or the mixture of gold nanoparticles and analytes were loaded into the capillary through atmospheric pressure. Because of the high capture efficiency associated with the micro/nanostructured channels,[30−32] the sample consumption required for SERS detection can be significantly reduced. In our experiments, only 2 μL of solution was used to flow through the capillary within 5 min. Figure 2 panels c and d show the typical scanning electron microscopy (SEM) images for gold nanoparticles adsorbed in the multihole capillary. Inside the flow channels, discrete gold nanoparticles were quite uniformly distributed on the surface area with a density of 6.1 $\pm$ 0.5 particles/μm^2, except a few sparked dimers or trimers.

The performance of the flow-through multihole capillary for Raman spectroscopy was then characterized with the well-studied molecular probe R6G dye. To fully attach R6G molecules to gold nanoparticles for enhancement, we mixed the R6G solution and gold nanoparticles solution with a predetermined ratio for several minutes before loading the mixture into the capillary, similar to others' work reported earlier.[4,6] This procedure made it easier for us to estimate the number of R6G molecules detected by using the number of gold nanoparticles within the laser probe area, under the assumption that R6G molecules and gold nanoparticles were stoichiometrically bound to each other.

Typical SERS spectra for R6G at the concentration of 5 $\times$ 10^{-7} M were taken stepwise at a 160 μm interval from the capillary head to a position 1.6 mm downstream, as plotted in Figure 3a. Distinctive Raman shifts at 785, 1206, 1319, 1369, and 1516 cm^{-1} were observed, which are associated with the characteristic vibration modes of a C−H band and an aromatic C−C stretching band of R6G, respectively.[37] Since nanoparticle transport is dominated by convection in the microfluidic channel,[38] the gold nanoparticle density adsorbed onto the PAH-modified channel surface gradually decreases along the flowing direction, as reflected by the gradually reduced SERS signal in Figure 3a,b. Note the decrease in the SERS intensity is monotonic without any abrupt change, suggesting that the SERS signal results mainly from discrete single nanoparticles rather than nanoclusters or aggregations, which would cause large fluctuations in the SERS intensity distribution along the capillary. All the results

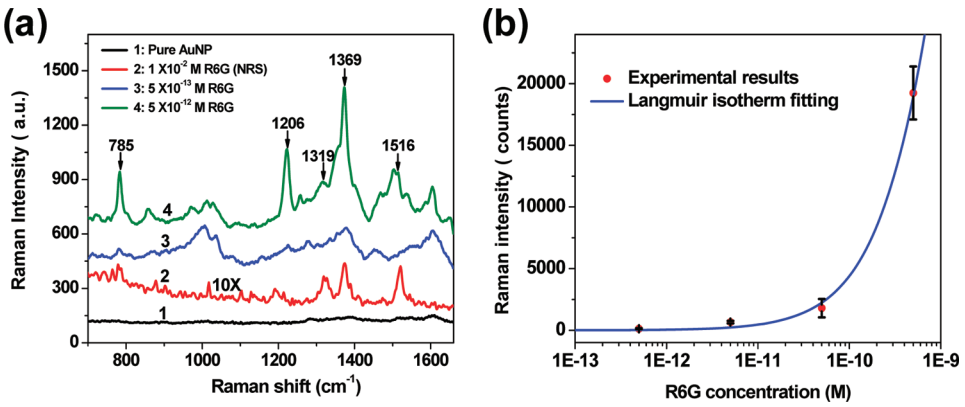

Figure 4. (a) SERS spectra of different concentrations of R6G (0, 5×10^{-13}, 5×10^{-12} M) using SERS-active capillary, and normal Raman spectrum (NRS) of 1×10^{-2} M R6G in solution in a glass cuvette (size: 10 mm × 10 mm × 10 mm) (with 10 times magnification). (b) SERS intensity at 1369 cm^{-1} for a series of concentrations of R6G from 5×10^{-13} M to 5×10^{-10} M. Error bars were obtained with at least three runs. The solid curve shows the Langmuir isotherm fit to the experimental data.

indicate that the gold nanoparticle functionalized multihole capillary has achieved large SERS-active surface area and reliable SERS-active sites for subsequent SERS detection.

To investigate the capability of the flow-through optofluidic SERS platform, we measured a series of low concentrations of R6G solutions from 5×10^{-10} M to 5×10^{-13} M, which were prepared by mixing the R6G solutions of 1×10^{-9} M to 1×10^{-12} M with 4.8×10^{9} particles/mL gold nanoparticle at a 1:1 ratio in volume, respectively. Assuming that all the R6G molecules are attached to the gold nanoparticles, the ratio between R6G molecules and gold nanoparticles is 125:1, 12.5:1, 1.25:1, 0.125:1 for the R6G concentration of 5×10^{-10} M, 5×10^{-11} M, 5×10^{-12} M, and 5×10^{-13} M, respectively. Note that each nanoparticle is expected to contain mostly zero or a few R6G molecules according to the Poisson distribution for those low R6G concentrations. On the basis of the gold nanoparticle density of 6.1 particles/μm^2 obtained previously, we estimate that 4.5×10^{3} gold nanoparticles are within the effective detection volume, corresponding to 5.6×10^{5}, 5.6×10^{4}, 5.6×10^{3}, and 560 R6G molecules, respectively, for the R6G concentrations mentioned above, which results in a much larger SERS signal than in the 2-D planar SERS detection.

Figure 4a shows the SERS spectra of R6G at concentrations of 5×10^{-12} and 5×10^{-13} M. For comparison, the SERS spectrum of pure gold nanoparticles in the absence of R6G and the normal Raman spectrum (NRS) of R6G at a concentration of 1×10^{-2} M in a 1-mL glass cuvette are also shown. The characteristic R6G peaks are clearly observed for 5×10^{-12} M, despite some differences from the normal Raman spectrum, which are expected as the interaction between the molecules and gold nanoparticles results in conformation changes and variations in molecular vibration modes. For R6G with the concentration of 5×10^{-13} M, although fewer than 600 R6G molecules are within the detection volume, according to the above calculation, the SERS peaks at 785 and 1369 cm^{-1} are still observable to indicate the presence of R6G molecules, attesting to the excellent sensing performance of the multihole capillary as the optofluidic SERS platform.

The enhancement factor (EF) of the proposed SERS system can be estimated using the following equation:[39]

$$\mathrm{EF} = (I_{\mathrm{SERS}}/I_{\mathrm{norm}})(N_{\mathrm{norm}}/N_{\mathrm{SERS}})$$

where I_{SERS} and I_{norm} are the measured Raman intensity for SERS and NRS, respectively. N_{norm} and N_{SERS} are the number of R6G molecules in the detection volume for NRS and SERS, respectively. We used the strongest signature stretching mode at 1369 cm^{-1} at 5×10^{-12} M for SERS and 1×10^{-2} M for NRS shown in Figure 4a. The number of R6G molecules detected is 5.6×10^{3} for 5×10^{-12} M solution in SERS and 5.1×10^{9} for 1×10^{-2} M solution in NRS. With 35 times higher SERS intensity than NRS intensity, the EF is calculated to be 3.2×10^{7}. Referring to our previous results,[36] we estimate that over 10^{6} fold enhancement results from the gold nanoparticle adsorbed on the capillary surface. Additional enhancement may be attributable to the light confinement and multiple surface reflections or scattering of the multihole capillary. To verify this, a control experiment was performed to measure the normal Raman spectra of 1×10^{-2} M R6G in the multihole capillary, which showed that over 20-fold enhancement in NRS could be achieved as compared to the same experiment performed using a 1-mL glass cuvette (see Figure S3 in Supporting Information).

The limit of detection (LOD) for the multihole capillary optofluidic SERS system was also evaluated by varying R6G concentrations, then measuring the intensity of characteristic R6G band at 1369 cm^{-1} at a position with maximum signal along the capillary (mostly close to the flow inlet), as plotted in Figure 4b. The experimental data were obtained using at least three independent capillaries for each concentration, achieving reliable measurements with less than 20% SERS

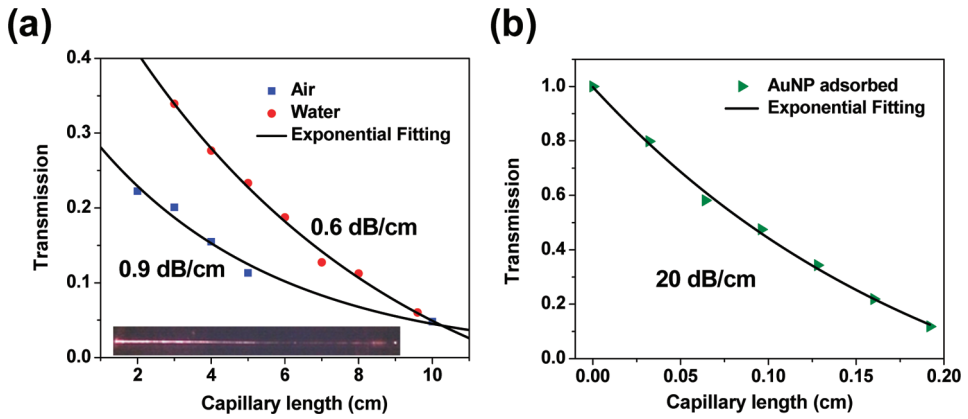

Figure 5. (a) Transmission loss for multihole capillary filled with air or water. The inset shows the picture of light propagating within the capillary. (b) Transmission loss for gold nanoparticle-functionalized multihole capillary.

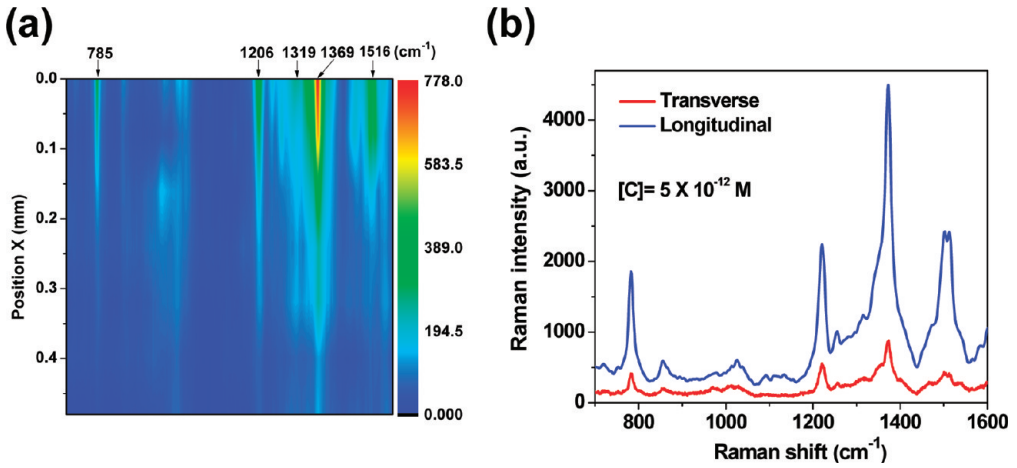

Figure 6. (a) SERS intensity distribution along the multihole capillary in the transverse direction. (b) Comparison of SERS intensity in the transverse and longitudinal detection using the same multihole capillary adsorbed with the mixture of R6G molecules and gold nanoparticles.

intensity variation. Moreover, it was well fit by a Langmuir isotherm curve with nonlinear least-squares regression.[37] By substituting three standard deviations of the blank signal into the fitted Langmuir isotherm curve, an estimated LOD of 70 fM is obtained, which is three orders of magnitude better than that achieved with a long PCF with discrete silver nanoparticles,[21,22] and similar to that in the nanoporous polymer monolith with silver nanoparticle aggregations.[29]

Longitudinal Detection. Apart from excellent performance achieved with the transverse direction, further improvement is possible with the longitudinal measurement by accumulating SERS intensity along the capillary. We first investigated the light guiding properties of the multihole capillary. As shown in the inset of Figure 5a, the light propagation can be observed along the capillary for a long distance of 10 cm (see also the images of the light coming out of the endface of a multihole capillary in Figure S4 in Supporting Information). Using the cut-back method with the same optical system, we measured the transmission loss to be 0.9 and 0.6 dB/cm for air and water filled capillary, respectively. Clearly, when the gold nanoparticles are adsorbed onto the inner surface of the capillary, the transmission loss is expected to be much larger due to the nature of absorption and scattering of the metallic nanoparticles. However, it is difficult to measure the transmission loss of a much shorter (~3 mm) capillary immobilized with gold nanoparticles using the cut-back method experimentally. Instead, we adopted an equivalent method, where we quantified the scattered light from the same excitation source (785 nm diode laser) at different locations of the capillary along the light propagation direction (see Figure S5 in Supporting Information). As expected, the transmission loss was dramatically increased to 20 dB/cm (see Figure 5b), similar to what was reported earlier.[35] Such a large transmission loss indicates that the multihole capillary allows large field-metal nanoparticle interaction for SERS enhancement.[22,35] The characteristic length for 3 dB loss is 1.50 mm, which implies that the proposed optofluidic SERS system is able to excite and collect the SERS with an effective length of 0.75 mm along the capillary. This effective length provides much larger

interaction area for signal accumulation than in the transverse direction.

To demonstrate the advantage of using the longitudinal detection, we used a 3-mm-long multihole capillary loaded with a 2 μL mixture with the final concentration of 5×10^{-12} M R6G and 2.4×10^9 particles/mL gold nanoparticles. We first measured the SERS intensity at several positions along the capillary using the transverse detection and found continuous SERS signal along the capillary (Figure 6a). Then we switched to measure the SERS intensity along the longitudinal direction. Even without optimization of the capillary (such as endface flatness) for better SERS collection efficiency, more than 5.5 times higher SERS signal was achieved than the maximum signal in the transverse direction (Figure 6b), which suggests that the capillary has the ability to accumulate SERS signal along the capillary length. The total EF in the longitudinal direction is estimated to be over 10^8, and the LOD is estimated to be 14 fM.

CONCLUSION

In summary, we have developed a novel optofluidic SERS-active platform using a flow-through multihole capillary, which provides a unique 3-D configuration for large SERS-active area, inherent fluidic channels for sample delivery, and well-defined structure for light guiding. It also allows for simple, costly effective fabrication, and low sample consumption. Moreover, ultrasensitive SERS detection with an enhancement factor of over 10^8 and a detection limit better than 100 fM for R6G molecules, has been achieved. Adjustments of experimental conditions, including the use of an excited laser source close to the resonances of analytes and metallic nanoparticles,[40] optimization of metallic nanoparticle density and the accumulation length,[23] and the use of modifications of the nanoparticle surfaces to enhance selected interactions between analytes and the sensor[41] are expected to yield further improvements in sensitivity and selectivity using the SERS-active multihole capillary. In addition, the optofluidic platform provides facile integration of the sensing elements into a range of capillary and microfluidic devices for bio/chemical detection. For example, integrating with the label-free biosensor demonstrated recently[30] can provide complementary information on molecular interaction.[42,43] We believe that the robust flow-through optofluidic SERS platform described here will drastically enhance the applicability of SERS-based biological and chemical detections.

MATERIALS AND METHODS

Materials. Gold(III) chloride solution (30 wt % of $HAuCl_4$ in dilute HCl), poly(allyamine hydrochloride) (PAH) (average molecular weight of 15000 g/mol), sulfuric acid (96.0%, Acros Organics, ACS reagent), were purchased from Sigma-Aldrich, USA. Sodium citrate (enzyme grade) was purchased from Fisher Scientific, USA. They were used without further purification. Milli-Q water was filtered by Quantum Ex, Ultrapure Oranex Cartridge (Millipore) filtration columns and used for all experiments. All glassware were cleaned overnight in the mixture solution prepared by dissolving 120 g of Nochromix (Godax Laboratories, Inc., MD, USA) powder in 3.78 L of concentrated sulfuric acid and were then thoroughly rinsed with Milli-Q water.

Fabrication and Treatment of the Multihole Capillary. The microstructured multihole capillary was fabricated using an in-house computer controlled fiber/capillary drawing system and a borosilicate glass preform obtained from Incom. Inc., Charlton, MA. Specially, the multihole capillary has 2700 uniform hexagonal holes with 18-μm hole size. Before pulling, the preform was treated with the following procedure: first illuminated under UV light for 1 h, then put in ethanol cleaning in ultrasound for 30 min, and illuminated under UV light for another 1 h. To keep a certain air pressure inside the channels, a piece of 5 cm long preform was used and sealed both ends using glue. Suitable heating time, feeding, and pulling speeds are chosen to pull a long-length and large surface-to-volume ratio capillary. The pulled capillary was treated with the same procedure as the preform before use. After treatment, a desirable length of capillary (such as 3 mm) was assembled into a flat-end needle. A PAH solution in water (0.05 mg/mL) was injected into the capillary with 0.01 mL/min for 20 min, and then Mill-Q water was continuously allowed to flow to thoroughly rinse the PAH-modified capillary so that the unbound and/or weakly adsorbed PAH molecules were completely removed from the multihole capillary.

Synthesis of Gold Nanoparticles. Gold nanoparticles were synthesized using a UV-assisted photochemical method as described in the previous report.[36] Briefly, to achieve gold nanoparticles which have an average size of 117 nm in diameter, a molar ratio of 1:1.7 for $HAuCl_4$ and sodium citrate were stirred for ~2 min and then placed under a UV lamp (Dymax 2000-EC UV curing light source flood lamp system). The sample was then under continuous stirring for 10 min until the color of the solution changed from yellow to reddish or orange.

System for Raman and SERS Measurements. Raman and SERS measurements were carried out with the customized Raman spectroscopy system, consisting of a 785 nm excitation laser (Process Instruments, PI-ECL-785-300-FC-SH) and a spectrometer (Horiba Scientific iHR550, focal length, 550 mm) equipped with a 600 grooves per mm grating and a spectroscopy grade CCD. An aspheric lens (NA = 0.55 and f = 4.51 mm) was used for delivery of the laser excitation and collection of the Raman signal. The excitation light was focused onto a spot of approximately 3 μm in diameter. All the Raman data were acquired with 6 mW excitation power and 2 s exposure time.

Supporting Information Available: Additional information and graphics as described in the text. This material is available free of charge *via* the Internet at http://pubs.acs.org.

REFERENCES AND NOTES

1. Fleischmann, M.; Hendra, P. J.; McQuillan, A. J. Raman Spectra of Pyridine Adsorbed at a Silver Electrode. *Chem. Phys. Lett.* **1974**, *26*, 163–166.
2. Jeanmaire, D. L.; Van Duyne, R. P. Surface Raman Spectroelectrochemistry: Part I. Heterocyclic, Aromatic, and Aliphatic Amines Adsorbed on the Anodized Silver Electrode. *J. Electroanal. Chem. Interfacial Electrochem.* **1977**, *84*, 1–20.
3. Kneipp, K.; Wang, Y.; Kneipp, H.; Perelman, L. T.; Itzkan, I.; Dasari, R. R.; Feld, M. S. Single Molecule Detection Using Surface-Enhanced Raman Scattering (SERS). *Phys. Rev. Lett.* **1997**, *78*, 1667.
4. Nie, S.; Emory, S. R. Probing Single Molecules and Single Nanoparticles by Surface-Enhanced Raman Scattering. *Science* **1997**, *275*, 1102–1106.

5. Baker, G. A.; Moore, D. S. Progress in Plasmonic Engineering of Surface-Enhanced Raman-Scattering Substrates toward Ultra-Trace Analysis. *Anal. Bioanal. Chem.* **2005**, *382*, 1751–1770.
6. Dieringer, J. A.; Wustholz, K. L.; Masiello, D. J.; Camden, J. P.; Kleinman, S. L.; Schatz, G. C.; Van Duyne, R. P. Surface-Enhanced Raman Excitation Spectroscopy of a Single Rhodamine 6G Molecule. *J. Am. Chem. Soc.* **2008**, *131*, 849–854.
7. Choi, C. J.; Xu, Z.; Wu, H.-Y.; Liu, G. L.; Cunningham, B. T. Surface-Enhanced Raman Nanodomes. *Nanotechnology* **2010**, *21*, 415301.
8. Li, W. D.; Ding, F.; Hu, J.; Chou, S. Y. Three-Dimensional Cavity Nanoantenna Coupled Plasmonic Nanodots for Ultrahigh and Uniform Surface-Enhanced Raman Scattering over Large Area. *Opt. Express* **2011**, *19*, 3925–3936.
9. Caldwell, J. D.; Glembocki, O.; Bezares, F. J.; Bassim, N. D.; Rendell, R. W.; Feygelson, M.; Ukaegbu, M.; Kasica, R.; Shirey, L.; Hosten, C. Plasmonic Nanopillar Arrays for Large-Area, High-Enhancement Surface-Enhanced Raman Scattering Sensors. *ACS Nano* **2011**, *5*, 4046–4055.
10. Chan, S.; Kwon, S.; Koo, T. W.; Lee, L. P.; Berlin, A. A. Surface-Enhanced Raman Scattering of Small Molecules from Silver-Coated Silicon Nanopores. *Adv. Mater.* **2003**, *15*, 1595–1598.
11. Jiao, Y.; Ryckman, J. D.; Ciesielski, P. N.; Escobar, C. A.; Jennings, G. K.; Weiss, S. M. Patterned Nanoporous Gold as an Effective SERS Template. *Nanotechnology* **2011**, *22*, 295302.
12. Zhang, L.; Lang, X.; Hirata, A.; Chen, M. Wrinkled Nanoporous Gold Films with Ultrahigh Surface-Enhanced Raman Scattering Enhancement. *ACS Nano* **2011**, *5*, 4407–4413.
13. Psaltis, D.; Quake, S. R.; Yang, C. Developing Optofluidic Technology through the Fusion of Microfluidics and Optics. *Nature* **2006**, *442*, 381–386.
14. Monat, C.; Domachuk, P.; Eggleton, B. J. Integrated Optofluidics: A New River of Light. *Nat. Photon* **2007**, *1*, 106–114.
15. Erickson, D.; Sinton, D.; Psaltis, D. Optofluidics for Energy Applications. *Nat. Photon.* **2011**, *5*, 583–590.
16. Schmidt, H.; Hawkins, A. R. The Photonic Integration of Non-solid Media Using Optofluidics. *Nat. Photon.* **2011**, *5*, 598–604.
17. Fan, X.; White, I. M. Optofluidic Microsystems for Chemical and Biological Analysis. *Nat. Photon.* **2011**, *5*, 591–597.
18. Yin, Y.; Qiu, T.; Zhang, W. J.; Chu, P. K. Recent Developments in Optofluidic-Surface-Enhanced Raman Scattering Systems: Design, Assembly, and Advantages. *J. Mater. Res.* **2011**, *26*, 170–185.
19. Amezcua-Correa, A.; Yang, J.; Finlayson, C. E.; Peacock, A. C.; Hayes, J. R.; Sazio, P. J. A.; Baumberg, J. J.; Howdle, S. M. Surface-Enhanced Raman Scattering Using Microstructured Optical Fiber Substrates. *Adv. Funct. Mater.* **2007**, *17*, 2024–2030.
20. Cox, F. M.; Argyros, A.; Large, M. C. J.; Kalluri, S. Surface Enhanced Raman Scattering in a Hollow Core Microstructured Optical Fiber. *Opt. Express* **2007**, *15*, 13675–13681.
21. Yang, X.; Shi, C.; Wheeler, D.; Newhouse, R.; Chen, B.; Zhang, J. Z.; Gu, C. High-Sensitivity Molecular Sensing Using Hollow-Core Photonic Crystal Fiber and Surface-Enhanced Raman Scattering. *J. Opt. Soc. Am. A* **2010**, *27*, 977–984.
22. Khaing Oo, M. K.; Han, Y.; Kanka, J.; Sukhishvili, S.; Du, H. Structure Fits the Purpose: Photonic Crystal Fibers for Evanescent-Field Surface-Enhanced Raman Spectroscopy. *Opt. Lett.* **2010**, *35*, 466–468.
23. Han, Y.; Tan, S.; Khaing Oo, M. K.; Pristinski, D.; Sukhishvili, S.; Du, H. Towards Full-Length Accumulative Surface-Enhanced Raman Scattering-Active Photonic Crystal Fibers. *Adv. Mater.* **2010**, *22*, 2647–2651.
24. Measor, P.; Seballos, L.; Yin, D.; Zhang, J. Z.; Lunt, E. J.; Hawkins, A. R.; Schmidt, H. On-Chip Surface-Enhanced Raman Scattering Detection Using Integrated Liquid-Core Waveguides. *Appl. Phys. Lett.* **2007**, *90*, 211107.
25. Ko, H.; Tsukruk, V. V. Nanoparticle-Decorated Nanocanals for Surface-Enhanced Raman Scattering. *Small* **2008**, *4*, 1980–1984.
26. Ko, H.; Chang, S.; Tsukruk, V. V. Porous Substrates for Label-free Molecular Level Detection of Nonresonant Organic Molecules. *ACS Nano* **2009**, *3*, 181–188.
27. Choi, I.; Huh, Y. S.; Erickson, D. Size-Selective Concentration and Label-free Characterization of Protein Aggregates Using a Raman Active Nanofluidic Device. *Lab Chip* **2011**, *11*, 632–638.
28. Wang, M.; Jing, N.; Chou, I. H.; Cote, G. L.; Kameoka, J. An Optofluidic Device for Surface Enhanced Raman Spectroscopy. *Lab Chip* **2007**, *7*, 630–632.
29. Liu, J.; White, I.; DeVoe, D. L. Nanoparticle-Functionalized Porous Polymer Monolith Detection Elements for Surface-Enhanced Raman Scattering. *Anal. Chem.* **2011**, *83*, 2119–2124.
30. Guo, Y.; Li, H.; Reddy, K.; Shelar, H. S.; Nittoor, V. R.; Fan, X. Optofluidic Fabry-Pérot Cavity Biosensor with Integrated Flow-through Micro-/Nanochannels. *Appl. Phys. Lett.* **2011**, *98*, 041104.
31. Escobedo, C.; Brolo, A. G.; Gordon, R.; Sinton, D. Flow-through *vs* Flow-over: Analysis of Transport and Binding in Nanohole Array Plasmonic Biosensors. *Anal. Chem.* **2010**, *82*, 10015–10020.
32. Yanik, A. A.; Huang, M.; Artar, A.; Chang, T.-Y.; Altug, H. Integrated Nanoplasmonic−Nanofluidic Biosensors with Targeted Delivery of Analytes. *Appl. Phys. Lett.* **2010**, *96*, 021101.
33. Eijkelenborg, M. V. Imaging with Microstructured Polymer Fibre. *Opt. Express* **2004**, *12*, 342–346.
34. Apetrei, A. M.; Phan Huy, M. C.; Belabas, N.; Levenson, J. A.; Moison, J.-M.; Dudley, J. M.; Mélin, G.; Fleureau, A.; Galkovsky, L.; Lempereur, S. A Dense Array of Small Coupled Waveguides in Fiber Technology: Trefoil Channels of Microstructured Optical Fibers. *Opt. Express* **2008**, *16*, 20648–20655.
35. Peacock, A. C.; Amezcua-Correa, A.; Yang, J.; Sazio, P. J.; Howdle, S. M. Highly Efficient Surface Enhanced Raman Scattering Using Microstructured Optical Fibers with Enhanced Plasmonic Interactions. *Appl. Phys. Lett.* **2008**, *92*, 141113.
36. Khaing Oo, M. K.; Chang, C. F.; Sun, Y.; Fan, X. Rapid, Sensitive DNT Vapor Detection with UV-Assisted Photo-Chemically Synthesized Gold Nanoparticle SERS Substrates. *Analyst* **2011**, *136*, 2811–2817.
37. Hildebrandt, P.; Stockburger, M. Surface-Enhanced Resonance Raman Spectroscopy of Rhodamine 6G Adsorbed on Colloidal Silver. *J. Phys. Chem.* **1984**, *88*, 5935–5944.
38. Piorek, B. D.; Lee, S. J.; Santiago, J. G.; Moskovits, M.; Banerjee, S.; Meinhart, C. D. Free-Surface Microfluidic Control of Surface-Enhanced Raman Spectroscopy for the Optimized Detection of Airborne Molecules. *Proc. Natl. Acad. Sci. U.S.A.* **2007**, *104*, 18898–18901.
39. Yu, H.-Z.; Zhang, J.; Zhang, H.-L.; Liu, Z.-F. Surface-Enhanced Raman Scattering (SERS) from Azobenzene Self-Assembled "Sandwiches". *Langmuir* **1998**, *15*, 16–19.
40. Lim, D. K.; Jeon, K. S.; Hwang, J. H.; Kim, H.; Kwon, S.; Suh, Y. D.; Nam, J. M. Highly Uniform and Reproducible Surface-Enhanced Raman Scattering from DNA-Tailorable Nanoparticles with 1-nm Interior Gap. *Nat. Nanotechnol.* **2011**, *6*, 452–460.
41. Galarreta, B. C.; Norton, P. R.; Lagugné-Labarthet, F. SERS Detection of Streptavidin/Biotin Monolayer Assemblies. *Langmuir* **2011**, *27*, 1494–1498.
42. Jiao, Y.; Koktysh, D. S.; Phambu, N.; Weiss, S. M. Dual-Mode Sensing Platform Based on Colloidal Gold Functionalized Porous Silicon. *Appl. Phys. Lett.* **2010**, *97*, 153125.
43. Meyer, S. A.; Le Ru, E. C.; Etchegoin, P. G. Combining Surface Plasmon Resonance (SPR) Spectroscopy with Surface-Enhanced Raman Scattering (SERS). *Anal. Chem.* **2011**, *83*, 2337–2344.